

# Mechanical Behaviour of Zirconia-Toughened Alumina Laminates with or without Y-PSZ Intermediate Layers

M.D. Barros<sup>1</sup>, P.L. Rachadel<sup>1</sup>, M.C. Fredel<sup>1</sup>, R. Janssen<sup>2</sup>, D. Hotza<sup>\*3</sup>

<sup>1</sup>Department of Mechanical Engineering, Federal University of Santa Catarina (UFSC), 88040–900, Florianópolis, SC, Brazil

<sup>2</sup>Institute of Advanced Ceramics, Hamburg University of Technology (TUHH), Denickestrasse 15, D-21073 Hamburg, Germany

<sup>3</sup>Department of Chemical Engineering, Federal University of Santa Catarina (UFSC), 88040–900, Florianópolis, SC, Brazil

received September 21, 2017; received in revised form October 23, 2017; accepted November 15, 2017

## Abstract

Zirconia-toughened alumina (ZTA) laminates with 5 vol% (95A) and 30 vol% (70A) of yttria-partially stabilized zirconia (Y-PSZ), as well as laminated composites with thick ZTA layers and thin Y-PSZ layers were developed and processed by means of tape casting followed by co-firing. The addition of 5 vol% Y-PSZ led to grain refinement, higher densification and an increase in mechanical properties compared to those of pure alumina. In contrast, the addition of 30 vol% Y-PSZ refined the alumina grains and formed clusters of zirconia. However, it promoted lower densification when compared to pure alumina and 95A. Nevertheless, mechanical strength increased in the 70A composites owing to the zirconia toughening mechanism. Laminated composites with intermediate Y-PSZ layers have shown thermal residual stresses after sintering as a result of the different coefficients of thermal expansion (CTE) of the components and higher performance in mechanical behaviour owing to compressive stresses in ZTA layers and to the zirconia toughening mechanism present in Y-PSZ thin layers and in ZTA with 30 vol% thick layers.

*Keywords:* ZTA, Y-PSZ, laminated composites, tape casting

## I. Introduction

Ceramic matrix composites (CMC) are developed to overcome the brittleness and low reliability of monolithic ceramic materials. The main advantages of these materials include high strength at high temperatures, low weight and flaw tolerance. Oxide/oxide composites additionally offer good stability against corrosive and oxidative environments. Although CMCs are promising thermostructural materials, their application is limited by the absence of adequate reinforcements, processing difficulties, durability and cost<sup>1,2</sup>.

Zirconia-toughened alumina (ZTA) was designed to substitute alumina in applications where higher fracture resistance is needed. This material consists of an alumina matrix in which zirconia particles are embedded. Mechanical properties as flexural strength, fracture toughness and fatigue resistance are enhanced mainly due to stress-induced zirconia phase transformation<sup>3–6</sup>. The transformation of tetragonal zirconia into monoclinic zirconia results in volume expansion (~4%) that acts contrary to crack propagation due to compressive stresses around the crack tip. Enhanced mechanical properties are directly related to the amount of zirconia added<sup>7,8</sup>. Another mechanism responsible for improved mechanical behaviour in ZTA is microcracking. Volume expansion causes tan-

gential stresses around transformed particles and induces crack nucleation in a matrix. The crack propagates until a transformed zirconia particle is found and then it is deflected, becoming a ramified crack. Transformability of zirconia depends on grain size, stabilizer type and amount, and sintering parameters. Internal residual stresses generated by different coefficients of thermal expansion may also affect the mechanical properties of ZTA<sup>9–11</sup>.

In this context, interfaces, brittle layers and residual stresses present in laminated ceramics can be used in an attempt to oppose crack growth and/or to develop a threshold strength<sup>12–18</sup>. This behaviour offers the opportunity for tailoring the mechanical properties based on stacking of layers of different thickness and composition in a suitable sequence<sup>19</sup>. Laminated composites can be manufactured by means of different processing routes, such as tape casting<sup>18,20,21</sup>, dip coating<sup>22</sup>, spin coating<sup>23</sup>, sequential slip casting<sup>19,24</sup>, electrophoretic deposition (EPD)<sup>25,26</sup> and colloidal techniques. Combined processing can be also used, such as tape casting with dip coating<sup>27</sup>, tape casting with EPD<sup>16</sup>, or tape casting with EPD and dip coating<sup>28</sup>.

Drastic increases in strength and especially in fracture toughness at room temperature have been achieved in alumina/zirconia laminar composites owing to various crack-shielding phenomena related to the presence of the layers (delamination, crack deflection, etc.)<sup>19</sup>. In particular,

\* Corresponding author: [d.hotza@ufsc.br](mailto:d.hotza@ufsc.br)

ceramic composites with a layered structure composed of alumina-zirconia have been reported to exhibit an increased apparent fracture toughness and energy absorption as well as non-catastrophic failure behaviour<sup>23,29</sup>. For strongly bonded multilayers, the elastic mismatch during sintering between adjacent layers – resulting from the difference in Young's moduli, thermal expansion coefficients, chemical reactions and/or phase transformations – generates residual stresses throughout the material. These residual stresses can be controlled in order to improve the mechanical properties<sup>30</sup>.

In this work, laminated ZTAs with 5 and 30 vol% yttria-partially stabilized zirconia (Y-PSZ) were produced by means of tape casting and their physical and mechanical properties were compared with those of pure alumina. Thereafter, laminated composites with thick ZTA layers and thin Y-PSZ interlayers were fabricated by means of tape casting, and the influence of toughening mechanisms and residual stresses induced by thick compressive layers and thin tensile layers on the mechanical behaviour of the composites was investigated.

## II. Materials and Methods

### (1) Preparation of alumina and ZTA samples

Starting powders were alumina (CT 3000 SG, Almatis,  $d_{50} = 0.40 \mu\text{m}$  and  $S_s = 7.60 \text{ m}^2/\text{g}$ ) and partially stabilized zirconia with 3 % mol  $\text{Y}_2\text{O}_3$  (Y-PSZ, TZ-3YB-E, Tosoh,  $d_{50} = 0.04 \mu\text{m}$  and  $S_s = 16 \pm 3 \text{ m}^2/\text{g}$ ), according to the respective suppliers. Three different suspensions were prepared with 25 vol% solids: 100A – composed of 100 vol%  $\text{Al}_2\text{O}_3$ ; 95A – with 95 vol%  $\text{Al}_2\text{O}_3$ , and 5 vol% Y-PSZ; and 70A – 70 vol%  $\text{Al}_2\text{O}_3$  and 30 vol% Y-PSZ.

First, the powder was deagglomerated in deionized water with addition of 1.5 wt% dispersant (ammonium salt of polymethacrylic acid, Darvan C-N, Vanderbilt) by means of ball milling for 24 h. Afterwards, 20 wt% binder (aqueous dispersion of styrene and acrylic acid esters, Clariant Mowilith LDM 6138), 1.5 wt% surfactant (coconut diethanolamide, Stepan) and 0.5 wt% antifoamer (30 % active silicone emulsion, Antifoam Y-30, Sigma-Aldrich) were added and the slurries were mixed in a ball mill for the next 30 min. All the weight percent are referred to solids content in the slurry. Finally, the suspensions were allowed to stand for 30 min to ensure the removal of any air bubbles.

The slurries were tape-cast using a stationary-blade/moving-carrier table-top tape-cast machine (CC-1200, Richard E. Mistler). Tapes were cast onto a silicone-coated carrier film (Mylar G10JRM, Richard E. Mistler) with casting speed of 6 cm/min and allowed to dry in air at ambient temperature ( $\sim 25 \text{ }^\circ\text{C}$ ) for 24 h. The gap between the blade and the carrier was set manually to obtain a final tape thickness of 90 to 200  $\mu\text{m}$ .

Lamination was performed in a warm press (20 MPa, 60  $^\circ\text{C}$ , 5 min) by stacking three green tapes between two metal plates. A Mylar G10JRM tape was set between metal plates and tapes to avoid adherence. Debinding and sintering were performed in an electrically heated furnace in air. The green laminates were debinded by heating up to 600  $^\circ\text{C}$  with a heating rate of 1 K/min and holding time of

1 h. The laminates were then heated up with the rate of 5 K/min and sintered at 1550  $^\circ\text{C}$ . After a holding time of 2 h, the laminates were cooled down to room temperature.

### (2) Characterization of alumina and ZTA samples

Microstructure and fracture analyses were conducted by means of scanning electron microscopy (TM 3030, Hitachi). Densities of the sintered tapes were measured with the Archimedes method in compliance with EN 623 – 2<sup>31</sup>. Vickers hardness was measured with a Vickers hardness tester (HMV Microhardness Tester) according to EN 843 – 4<sup>32</sup> with load of 10 N (HV 1.0) over 15 s.

Three-point bending tests were performed with a universal test machine (EMIC) with capacity of 20 kN, following the EN 843 – 1<sup>33</sup> norm. A total of 35 samples measuring 60 mm  $\times$  10 mm  $\times$  0.3 mm were manufactured and tested as-sintered. A load cell with 100 N capacity and load speed of 0.5 mm/min was used. The distances between the rollers were set with 42 mm. The data were analysed according to the EN 843 – 5<sup>34</sup> norm, using Weibull analysis.

### (3) Preparation of laminated composites

Additionally, laminated composites of thick ZTA (95A and 70A) layers and thin Y-PSZ layers were fabricated. Thin layers were also produced by means of tape casting using the same method for the preparation of the slurry, which was prepared with 18 vol% Y-PSZ, 2.5 wt% dispersant, 60 wt% binder, 3.5 wt% surfactant and 1.5 wt% antifoamer. All wt% is referred to solids content in the slurry. The slurry was cast using the same parameters set as reported before. Next, the composite was laminated by stacking the two thin layers between three thick layers. The thick layers were composed of three tapes, while the thin layer was composed of one tape, as shown in Fig 1.

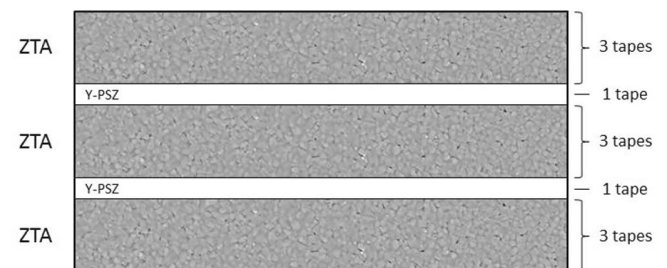


Fig. 1: Scheme of laminated composite formed by thick ZTA layers and thin Y-PSZ layers.

Samples with thin Y-PSZ layers and thick 95A layers were called 95AZ. Samples with thin Y-PSZ layers and thick 70A layers were called 70AZ. Thermal treatment and sintering followed the same steps as applied for the ZTA samples.

### (4) Characterization of laminated composites

SEM was used to analyse the microstructure and fracture sections of composites. Three-point bending tests were conducted<sup>35</sup>, with ten as-sintered composite samples measuring 60 mm  $\times$  10 mm  $\times$  1 mm, in compliance with EN 658 – 3<sup>36</sup> with further Weibull analysis.

Surface fracture was analysed by means of X-ray diffraction (XRD) to determine the crystal structure (Philips X’Pert) using 40 kV, 30 mA, and CuK $\alpha$  radiation. The diffraction patterns were measured at room temperature for diffraction angles  $2\theta$  between  $3^\circ$  and  $90^\circ$  with step size of  $0.02^\circ$ .

Residual stresses for a multi-layered system composed of  $n$  layers of material  $x$  and thickness  $t_x$  and  $n-1$  layers of material  $y$  and thickness  $t_y$  were estimated based on Eq. 1 and Eq. 2 <sup>37</sup>:

$$\sigma_x = \Delta\varepsilon \cdot E'_x \cdot \left( 1 + \frac{t_x E'_x n_x}{t_y E'_y n_y} \right)^{-1} \quad (1)$$

$$\sigma_y = \Delta\varepsilon \cdot E'_y \cdot \left( 1 + \frac{t_y E'_y n_y}{t_x E'_x n_x} \right)^{-1} \quad (2)$$

where  $\Delta\varepsilon$  is the difference in thermal strain between adjacent layers and  $E' = E_i / (1 - \nu_i)$ ,  $E_i$  being the Young’s modulus and  $\nu_i$  the Poisson’s ratio of a given layer.

### III. Results and Discussion

#### (1) Alumina and ZTA

Fig. 2 shows SEM micrographs of the surfaces of 100A, 95A and 70A samples. The final thickness of the samples was  $380 \pm 50 \mu\text{m}$  for 100A,  $390 \pm 80 \mu\text{m}$  for 95A and  $250 \pm 30 \mu\text{m}$  for 70A. It is observed that 100A presents an irregular grain size throughout the sample, with some larger grains. The average grain size of the alumina grains is  $1.2 \pm 0.5 \mu\text{m}$ . Otherwise, the 95A samples show uniform alumina grain size with dimensions comparable with the smaller grains of 100A. The average grain sizes of alumina and Y-PSZ are  $0.8 \pm 0.4 \mu\text{m}$  and  $0.4 \pm 0.1 \mu\text{m}$ , respectively. It is noted that the presence of 5 vol% Y-PSZ inhibits alumina grain growth and promotes grain refinement. Y-PSZ inclusions are located at grain boundaries, the vast majority at triple points, as a result of the densification process during sintering. Moreover, it is seen that the 70A samples present alumina grain sizes smaller than those in 95A owing to contact restriction of the alumina grains by the amount of zirconia, which forms clusters through the microstructure. The average grain sizes of alumina and Y-PSZ are  $0.6 \pm 0.2 \mu\text{m}$  and  $0.6 \pm 0.1 \mu\text{m}$ , respectively. As

shown, the average grain size of the zirconia for 70A is higher than for 95A owing to the smaller diffusion path and the presence of clusters.

Although the solubility of yttria in alumina is low ( $< 10 \text{ ppm}$ ), it may also avoid alumina grain growth. Yttrium ions, which are much larger than aluminium ions, tend to segregate at alumina grain boundaries, decreasing the elastic deformation energy and blocking ion diffusion through grain boundaries <sup>3</sup>. Table 1 lists the apparent density ( $\rho_a$ ), relative density ( $\rho_r$ ), and Vickers hardness ( $HV$ ) of 100A, 95A and 70A samples.

**Table 1:** Apparent density, relative density, and Vickers hardness of samples 100A, 95A and 70A.

	$\rho_a \text{ (g/cm}^3\text{)}$	$\rho_r \text{ (\%)}$	$HV \text{ (GPa)}$
100A	$3.85 \pm 0.02$	98.6	$17.88 \pm 0.32$
95A	$4.00 \pm 0.04$	99.6	$17.18 \pm 0.17$
70A	$4.46 \pm 0.07$	97.9	$15.56 \pm 0.58$

The theoretical density was determined based on the rule of mixtures. As a result, the higher the amount of zirconia, the higher the theoretical density. When 95A is compared with 100A, it can be observed that the relative density is higher for 95A. The Y-PSZ average particle size is smaller than the alumina average particle size, which indicates that zirconia fills the intergranular positions of alumina after sintering, becoming dispersed in the matrix and controlling grain growth. The relative density for 70A is the lowest. This result can be associated with the formation of clusters by zirconia, since these agglomerates prevent filling of the voids left by the alumina. The higher amount of organic additives used in the 70A slurry also induces a higher porosity and less densification. Table 1 also shows the values of Vickers hardness HV 1, with a test force of 9.807 N resulting from a mass of 1 kg.

It is observed that the higher the Y-PSZ amount, the lower the hardness, as the hardness follows the rule of mixture <sup>38</sup>. The literature shows values of 17–18 GPa for alumina and 12–13 GPa for zirconia <sup>39</sup>.

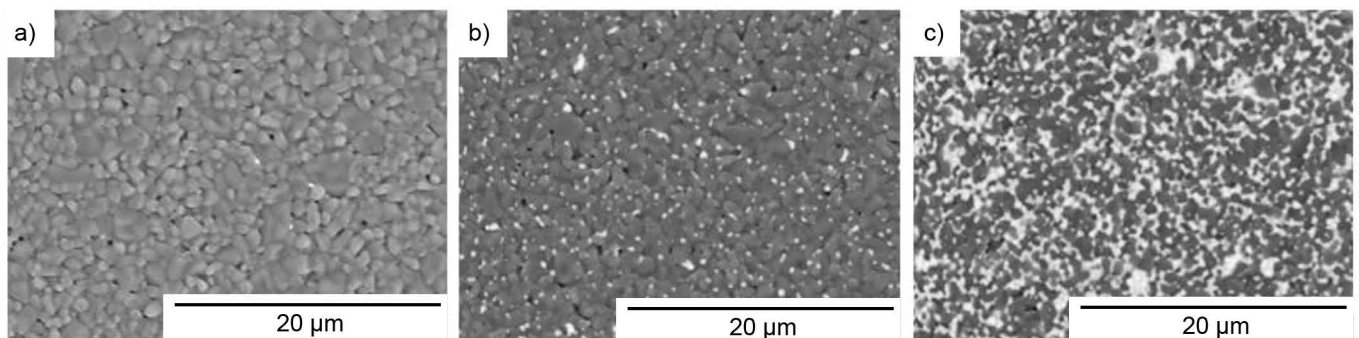


**Fig. 2:** SEM micrographs of surfaces of (a) 100A, (b) 95A and (c) 70A. Dark grains are alumina, while light grains are Y-PSZ.

Fig. 3 shows the Weibull analysis performed from flexural tests results, complemented by information given in Table 2. When 95A is compared with 100A, an increase in flexural strength ( $\sigma_f$ ), mean characteristic strength ( $\sigma_0$ ), Weibull modulus ( $m$ ) and coefficient of determination ( $R^2$ ) is observed. This can be explained by the higher relative density and the refined structure of 95A owing to the addition of 5 vol% Y-PSZ. According to the literature<sup>40</sup>, the mechanical strength of ceramics is inversely proportional to grain size square root.

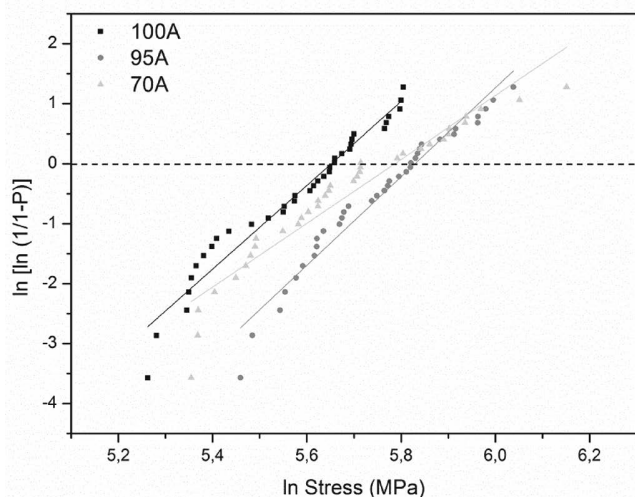


Fig. 3: Weibull analyses for 100A, 95A and 70A materials using the results obtained with flexural test for 35 samples of each composition.

70A samples present a higher flexural strength; however, the value of mean characteristic strength is between the values for 100A and 95A. The higher flexural strength can be related to the high presence of Y-PSZ promoting toughening by means of phase transformation. It is worth mentioning that the lower relative density of 70A can also act as a strength reducer.

To further understand the results related to the 70A samples found in Fig. 3 and Table 2, the surface of these composites was analysed with SEM. Fig. 4 shows the presence of expressive defects at the surface of samples at a size magnitude of 50 to 100  $\mu\text{m}$ . These defects probably originate from tape casting or lamination, and can be associated with the lower values found for mean characteristic strength and Weibull modulus, resulting in a decrease in the flexural strength and reliability of the composite.

Table 2: Flexural strength, mean characteristic strength, Weibull modulus and coefficient of determination for 100A, 95A and 70A samples.

	$\sigma_f$ (MPa)	$\sigma_0$ (MPa)	$m$	$R^2$
100A	331.7	284.7	6.9	0.9557
95A	419.2	340.0	7.3	0.9573
70A	469.1	325.8	5.3	0.9136

Moreover, all samples were tested as sintered. The lack of surface finishing can significantly reduce the flexural strength as in surface finishing material is removed and, consequently, the size of critical defects located at the surface is modified. Previous studies<sup>3</sup> have observed that surface finishing increases flexural strength by 20 % for alumina samples and 60 % for alumina/5 vol% of tetragonal zirconia. Fig. 5 shows the fracture section of the three samples in longitudinal and transversal directions.

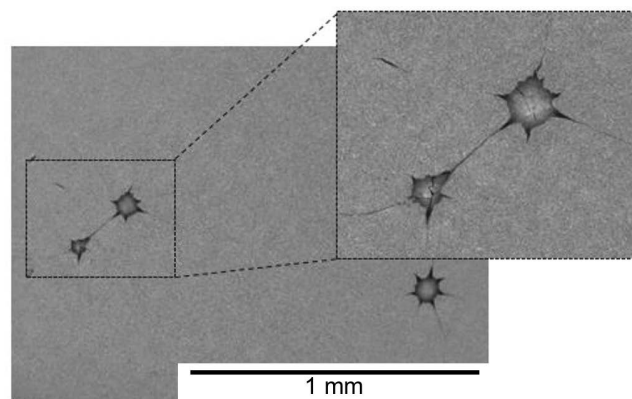


Fig. 4: SEM micrographs of 70A samples surface. Defect sizes from processing of 50 to 100  $\mu\text{m}$  can be observed.

A typical brittle fracture surface can be observed, as well as the predominance of intergranular fracture with a few regions of transgranular fracture, especially in 100A samples owing to the higher alumina grain size and lower flexural strength. The presence of intragranular pores is not observed. Nonetheless, intergranular pores with round and slit shape can be seen (Figs. 2a, 2b, 2c) that may act as defects and a limiting factor for the strength.

The paths of material cracks originating from a Vickers indentation are compared in Fig. 6. For 100A the cracks show a tortuous path with few deviations and higher angles. With the addition of 5 vol% Y-PSZ into the alumina matrix, the tortuosity (deviation angles) of the crack path decreases, since the alumina grain size decreases. Consequently, the cracks tend to follow the alumina grain boundaries. The average length of linear segments decreases and the number of deviations increases with the decrease of alumina grain size. The same is observed for the 70A samples where the alumina grains are even smaller. Although, when the crack passes through zirconia grain linear segments, few or no deflections are observed, indicating that phase transformation hinders crack propagation, but does not deflect it.

## (2) Laminated composites

Fig. 7 shows the SEM micrographs of 95AZ and 70AZ samples in transversal section. Thereby, 95A and 70A correspond to the thick layers and Y-PSZ to the thin bright layers. The thickness obtained for the samples are  $1100 \pm 100 \mu\text{m}$  for 95AZ, and  $700 \pm 100 \mu\text{m}$  for 70AZ. The laminates present the thin Y-PSZ layers well bonded to thick layers. No defects or delamination are observed along the interfaces.

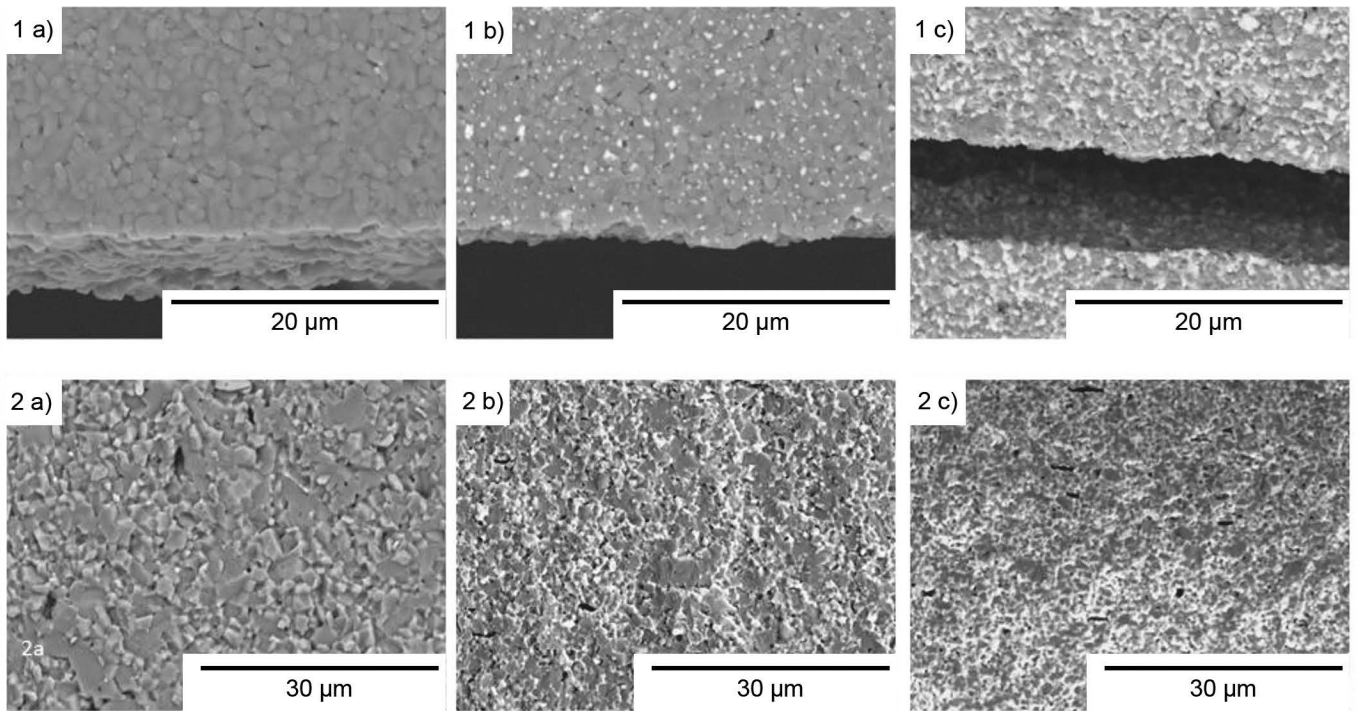


Fig. 5: Micrographs of: longitudinal (1) and transversal (2) fracture section of (a) 100A, (b) 95A and (c) 70A samples.

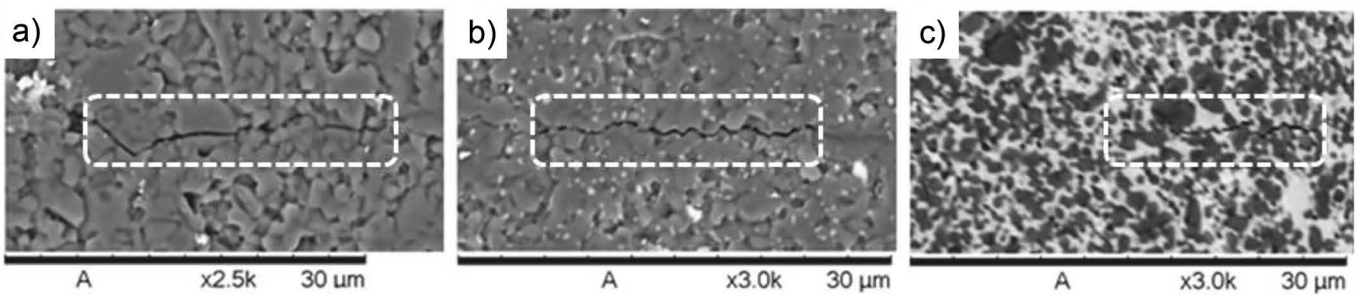


Fig. 6: SEM micrographs of cracks originating from Vickers indentation showing the crack path analysed for: (a) 100A, (b) 95A and (c) 70A.

Table 3 shows the values for the thickness obtained for thick ZTA layers ( $t_{ZTA}$ ) and thin Y-PSZ layers ( $t_Z$ ), and the ratio between them ( $R = t_{ZTA}/t_Z$ ). It also shows the values of residual stresses in each layer according to Eq. 1 and Eq. 2. Positive stresses are related to tensile stresses while negative stresses are related to compressive stresses. Thermal residual stresses were already expected owing to the different coefficient of thermal expansion (CTE) of alumina and zirconia. According to the layout of the composite, after sintering, the thick layers of ZTA should be under compressive stresses and the thin Y-PSZ layers should be under tensile stresses. Thick layers have a lower CTE compared to thin layers owing to the major presence of alumina. Therefore, the Y-PSZ layer demonstrates higher shrinkage during cooling as it has a higher CTE ( $\alpha_{Y-PSZ} > \alpha_{alumina}$ )<sup>41</sup>. As the interfaces are well-bonded, Y-PSZ layer is prevented from retracting, leading to biaxial residual stresses.

High values are observed for tensile stresses in Y-PSZ layer and low values for compressive stress in ZTA layers. This behaviour is highly influenced by the layer thickness. ZTA layers are considerably thicker than Y-PSZ layers and, consequently, they induce high stress while Y-PSZ

layers induce low stress. Higher values of R will show an increase of Y-PSZ residual stress and a decrease of ZTA stress.

Table 3: Thickness of ZTA and Y-PSZ layers, ratio between them and thermal residual stresses calculated for 95AZ and 70AZ samples.

	$t_{ZTA}$ ( $\mu\text{m}$ )	$t_Z$ ( $\mu\text{m}$ )	R	$\sigma_{t_{ZTA}}$	$\sigma_{t_Z}$
95AZ	$308 \pm 23$	$48.8 \pm 0.5$	6.3	-68.5	+639.1
70AZ	$200 \pm 9$	$55.3 \pm 1.5$	3.6	-82.5	+447.3

The composition of ZTA also influences the residual stresses. Composites with ZTA composed of 95A present higher tensile stress in zirconia layers than composites produced with 70A ZTA. 95A has higher alumina content than 70A. Accordingly, the CTE of 95A is lower than 70A and, consequently,  $\Delta\epsilon$  is higher.

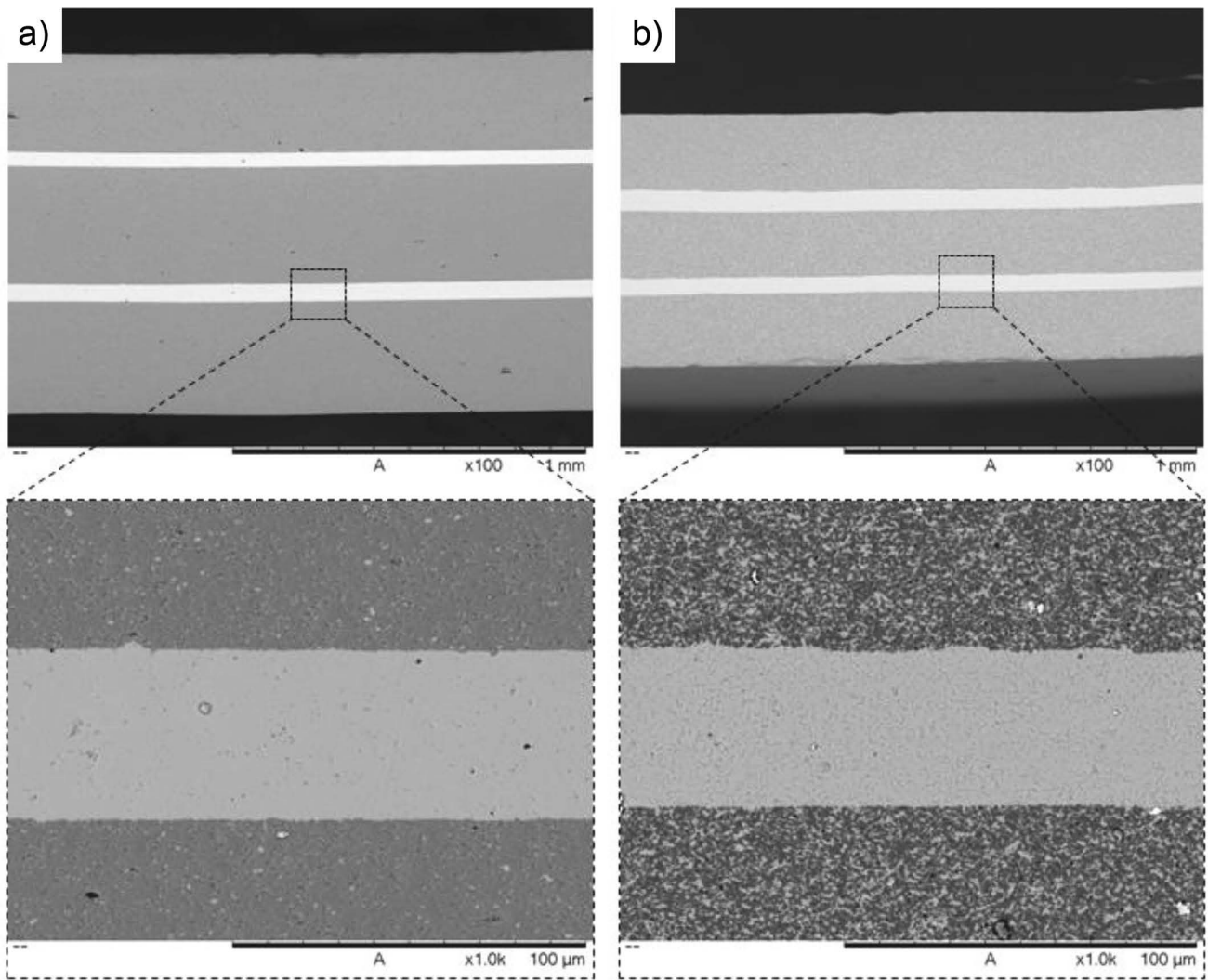


Fig. 7: SEM micrographs of transversal sections of (a) 95AZ and (b) 70AZ. Dark layers are ZTA while light layers are Y-PSZ.

Fig. 8 shows the results of laminated composites subjected to flexural tests with Weibull statistical analysis. In order to compare the results obtained for the laminated composites, samples with nine tapes of each ZTA were fabricated and tested. Additional information is given in Table 4. When the results of 95A and 70A (Table 4) and the previous flexural test using three tapes of each composition (Table 2) are compared, it is observed that a decrease in the flexural and mean characteristic strengths is related to the increase in sample volume, from three to nine stacked tapes. Therefore, the probability of finding a critical defect is higher and the material strength becomes lower for the thicker laminate.

In contrast to the previous flexural test using three tapes (Table 2), here the mean characteristic strength and Weibull modulus of 70A are higher than those of 95A. This is directly connected with the absence of critical defects on the surface observed for 70A samples (Fig. 9), which is the opposite trend when compared to the previously observed effect of external factors during tape casting (e.g. room temperature, impurities) or lamination (Fig. 4).

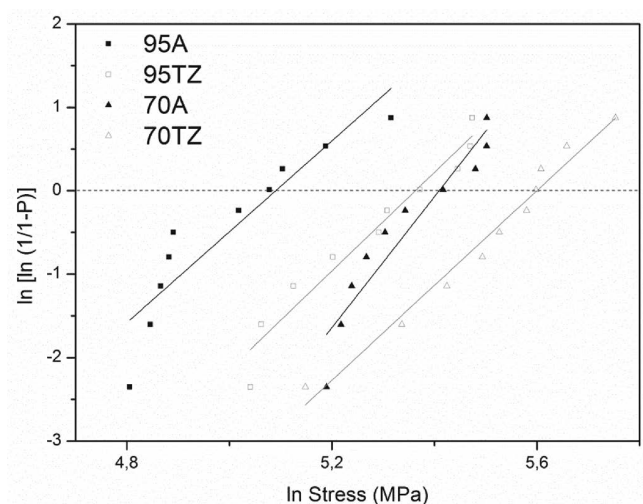


Fig. 8: Weibull analyses for 95A, 95AZ, 70A and 70AZ from flexural test, values for ten samples of each composition.

In general, the reinforcement layers enhance the mechanical properties of the material, increasing the flexural strength and mean characteristic strength. Although there are tensile stresses acting in Y-PSZ, the zirconia toughening mechanism controls the system and manages to exert a

positive influence on the mechanical strength of the composite. Hence, compressive ZTA layer also plays an important role in increasing mechanical strength. Finally, better results were achieved using 70A owing to the presence of zirconia toughening mechanism that may occur at the thick layer.

**Table 4:** Flexural strength, mean characteristic strength, Weibull modulus and coefficient of determination for 95A, 95AZ, 70A and 70AZ samples.

	$\sigma_f (MPa)$	$\sigma_0 (MPa)$	$m$	$R^2$
95A	203.4	162.4	5.4	0.8292
95AZ	238.3	213.3	5.9	0.9444
70A	245.1	223.4	7.8	0.8905
70AZ	315.1	270.3	5.6	0.9716

Fig. 10 shows the fracture surface of a transversal section of 95AZ and 70AZ composites. Typical brittle fracture can be noticed, with predominance of intergranular fracture and some transgranular fracture. Likewise, a high porosity is observed in Y-PSZ thin layers. This can be attributed to the high amount of organic additives used in the slur-

ries, which leave more voids when burned out, hindering in this way material densification. One alternative for improving this behaviour can be increasing the solid fraction and decreasing the amount of organics in Y-PSZ slurry.

Fig. 11 shows the XRD patterns of 70A and 70AZ fracture surfaces. The samples present  $\alpha$ -alumina, tetragonal zirconia and monoclinic zirconia. The presence of monoclinic phase of zirconia, characterized by peaks with  $2\theta$  angles of  $28.19^\circ$  and  $31.48^\circ$ , indicates that stress-induced phase transformation during crack occurs and increases the mechanical strength of both materials, although monoclinic zirconia resulting from spontaneous transformation may also exist. Fig. 12 displays the fracture surface of a longitudinal section of 95AZ and 70AZ composites. It is observed that points of the crack are deflected by delamination. This acts as a toughening mechanism, deflecting the crack and increasing its path until fracture. No crack deflection is observed through the interfaces and through Y-PSZ, indicating that the interfaces are well-bonded and that Y-PSZ layer does not act as a brittle layer. It is worth mentioning that crack path changes direction in ZTA layers near the interfaces. This fact is in line with the idea that residual stresses are higher near the interfaces and that compressive layers change the direction of a crack during its propagation.

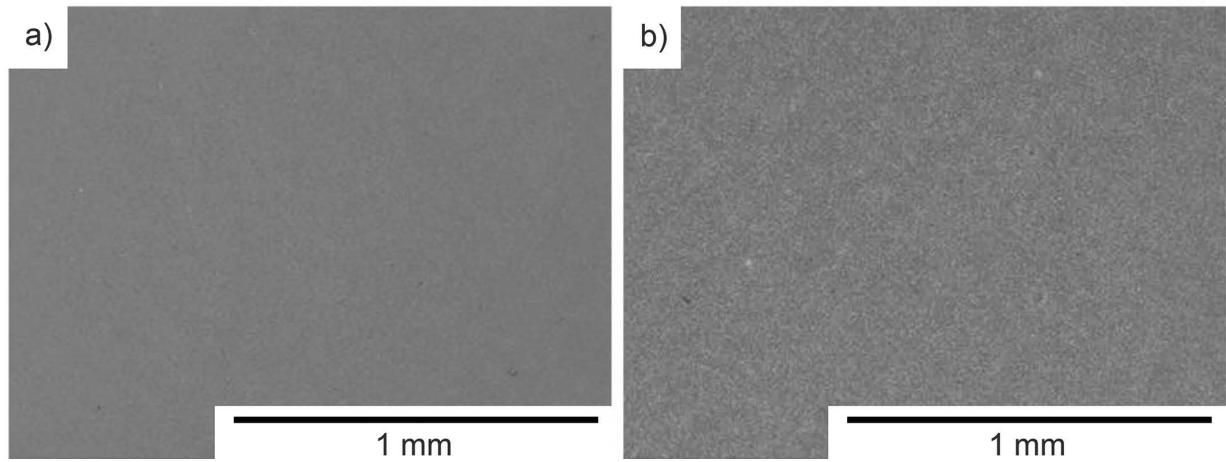


Fig. 9: SEM micrographs of (a) 95AZ surface and (b) 70AZ surface showing no critical defects for both samples.

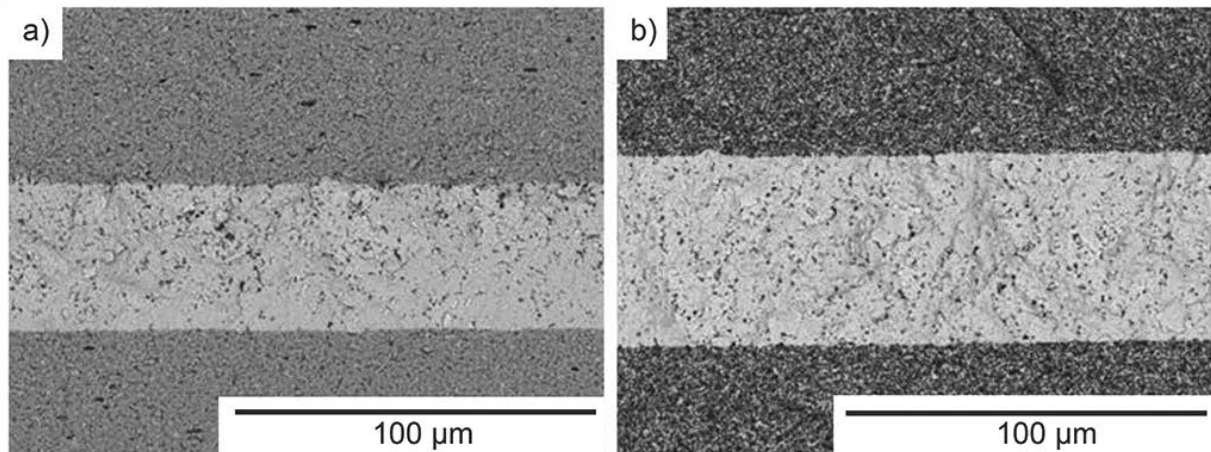


Fig. 10: Transversal fracture section of (a) 95AZ and (b) 70AZ samples.

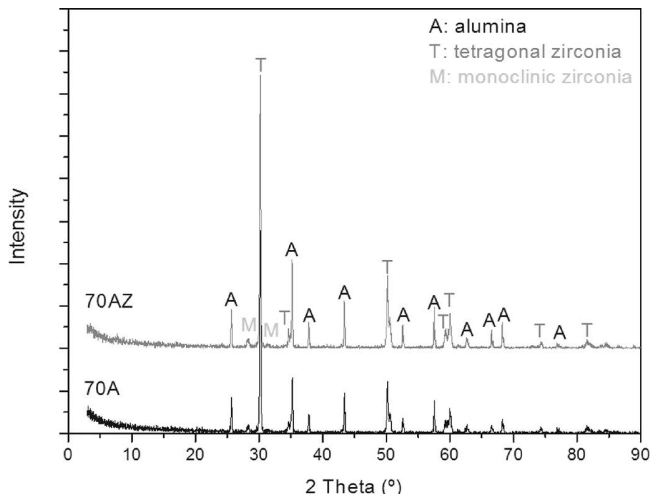


Fig. 11: XRD patterns of 70A and 70AZ.

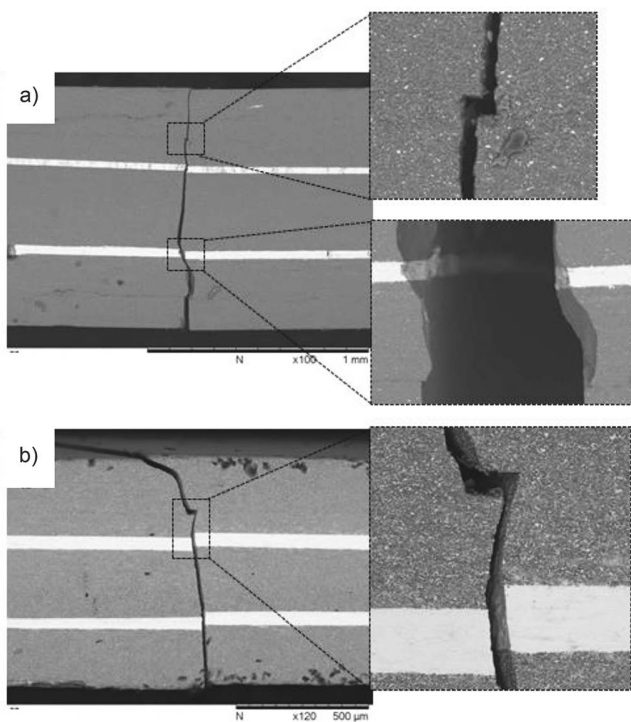


Fig. 12: Longitudinal fracture section of (a) 95AZ and (b) 70AZ samples.

#### IV. Conclusions

The addition of 5 vol% Y-PSZ inhibits alumina grain growth and promotes grain refinement. It also enhances densification because Y-PSZ particles fill intergranular positions of alumina. The addition of 30 vol% Y-PSZ restricts alumina grain growth and forms Y-PSZ clusters along the microstructure. Densification is lower than for the alumina samples because zirconia not only fills alumina voids, but forms clusters, too. The higher amount of organic additives used in the 70A slurries induces higher porosity and lower densification.

Hardness decreases with the addition of zirconia following the rule of mixtures. Flexural tests showed that grain refinement in 95A samples increased the mechanical properties and reliability when compared to 100A. 70A sam-

ples showed higher values for flexural strength than 95A, although the values of mean characteristic strength and Weibull modulus were less than the expected owing to surface defects in the 70A samples.

Laminated composites present higher residual stress in Y-PSZ thin layers (tensile stresses) than in ZTA thick layers (compressive stresses); this is directly related to the ratio between the layers' thickness. The composition of the ZTA layers also has an influence on residual stresses owing to changes in  $\Delta\epsilon$ . The reinforcement layer enhances the mechanical properties of the material and, although there are tensile stresses acting in Y-PSZ, the zirconia toughening mechanism exerts a positive effect on the mechanical strength of the composites. The compressive ZTA layer may be responsible for the increased strength. The 70A samples achieved better results for their mechanical properties owing to the presence of the zirconia toughening mechanism also occurring at the thick layer.

Fracture micrographs have shown a composite with strong interfaces and well-bonded layers. High porosity of the Y-PSZ thin layers was observed owing to the high amount of organic additives. In conclusion, even under tensile stress, the thin Y-PSZ layers may act as a toughening mechanism and hinder crack propagation. In addition, the composite is reinforced with thick ZTA layers under compressive stress. This, besides avoiding crack propagation by the residual stress, can generate mechanisms of energy dispersion (e.g. crack bifurcation).

#### Acknowledgements

The support of the Brazilian agencies CAPES and CNPq and the German DAAD is gratefully acknowledged.

#### References

- Volkman, E., Tushtev, K., Koch, D., Wilhelmi, C., Göring, J., Rezwani, K.: Assessment of three oxide/oxide ceramic matrix composites: mechanical performance and effects of heat treatments, *Compos. Part A Appl. Sci. Manuf.*, **68**, 19–28, (2015).
- Bansal, N.P., Lamon, J.: Ceramic matrix composites: Materials, modeling and technology. 2015.
- Tuan, W.H., Chen, R.Z., Wang, T.C., Cheng, C.H., Kuo, P.S.: Mechanical properties of  $\text{Al}_2\text{O}_3/\text{ZrO}_2$  composites, *J. Eur. Ceram. Soc.*, **22**, [16], 2827–2833, (2002).
- Shin, Y., Rhee, Y., Kang, S.: Experimental evaluation of toughening mechanisms in Alumina-Zirconia composites, *J. Am. Ceram. Soc.*, **82**, [5], 1229–1232, (1999).
- Karihaloo, B.L.: Contribution of  $t \rightarrow m$  phase transformation to the toughening of ZTA, *J. Am. Ceram. Soc.*, **74**, [7], 1703–1706, (1991).
- Lange, F.F.: Transformation toughening: part 4 – fabrication fracture toughness and strength of  $\text{Al}_2\text{O}_3\text{-ZrO}_2$  composites, *J. Mater. Sci.*, **17** 247–254, (1982).
- Green, D.J., Hannink, R.H.J., Swain, M.V.: Transformation toughening of ceramics, Boca Raton, FL. CRS Press. Inc, 232 (1989).
- Stevens, R.: An introduction to zirconia, Magnesium Elektron Publication No. 113, Stoke on Trent, UK, Sherwin Rivers (1983).
- Casellas, D., Nagl, M.M., Llanes, L., Anglada, M.: Growth of small surface indentation cracks in alumina and zirconia toughened alumina, *Key Eng. Mater.*, **127–131**, 895–902, (1997).
- Wang, J., Stevens, R.: Zirconia-toughened alumina (ZTA) ceramics, *J. Mater. Sci.*, **24**, [10], 3421–3440, (1989).

- 11 Evans, A.G., Cannon, R.M.: Toughening of brittle solids by martensitic transformations, *Acta Metall.*, **34**, [5], 761–800, (1986).
- 12 Gurauskis, J., Sánchez-Herencia, A.J., Baudín, C.: Alumina-zirconia layered ceramics fabricated by stacking water processed green ceramic tapes, *J. Eur. Ceram. Soc.*, **27**, [2–3], 1389–1394, (2007).
- 13 Clegg, W.J., Kendall, K., Alford, N.M., Button, T.W., Birchall, J.D.: A simple way to make tough ceramics, *Nature*, **347**, [6292], 455–457, (1990).
- 14 Ma, J., Wang, H., Weng, L., Tan, G.E.B.: Effect of porous interlayers on crack deflection in ceramic laminates, *J. Eur. Ceram. Soc.*, **24**, [5], 825–831, (2004).
- 15 Bueno, S., Baudín, C.: Design and processing of a ceramic laminate with high toughness and strong interfaces, *Compos. Part A Appl. Sci. Manuf.*, **40**, [2], 137–143, (2009).
- 16 Ferrari, B., Bartret, A., Baudín, C.: Sandwich materials formed by thick alumina tapes and thin-layered alumina-aluminium titanate structures shaped by EPD, *J. Eur. Ceram. Soc.*, **29**, [6], 1083–1092, (2009).
- 17 Bueno, S., Moreno, R., Baudín, C.: Design and processing of  $\text{Al}_2\text{O}_3\text{-Al}_2\text{TiO}_5$  layered structures, *J. Eur. Ceram. Soc.*, **25**, [6], 847–856, (2005).
- 18 Zhang, J.X., Jiang, D.L., Qin, S.Y., Huang, Z.R.: Fracture behavior of laminated SiC composites, *Ceram. Int.*, **30**, [5], 697–703, (2004).
- 19 Jiménez-Melendo, M., Gutiérrez-Mora, F., Domínguez-Rodríguez, A.: Effect of layer interfaces on the high-temperature mechanical properties of alumina/zirconia laminate composites, *Acta Mater.*, **48**, [18], 4715–4720, (2000).
- 20 Quinn, G.D., Melandri, C., De Portu, G.: Edge chipping resistance of alumina/zirconia laminates, *J. Am. Ceram. Soc.*, **96**, [7], 2283–2291, (2013).
- 21 Kuo, D., Kriven, W.M.: A strong and damage-tolerant oxide laminate, *J. Am. Ceram. Soc.*, **80**, [9], 2421–2424, (1997).
- 22 Sánchez-Herencia, A.J.: Water based colloidal processing of ceramic laminates, *Key Eng. Mater.*, **333**, 39–48, (2007).
- 23 Marshall, D.B., Ratto, J.J., Lange, F.F.: Enhanced fracture toughness in layered microcomposites of ce-zrO<sub>2</sub> and Al<sub>2</sub>O<sub>3</sub>, *J. Am. Ceram. Soc.*, **74**, [12], 2979–2987, (1991).
- 24 Bermejo, R., Torres, Y., Sánchez-Herencia, A.J., Baudín, C., Anglada, M., Llanes, L.: Residual stresses, strength and toughness of laminates with different layer thickness ratios, *Acta Mater.*, **54**, [18], 4745–4757, (2006).
- 25 Hadraba, H., Klimes, J., Maca, K.: Crack propagation in layered Al<sub>2</sub>O<sub>3</sub>/ZrO<sub>2</sub> composites prepared by electrophoretic deposition, *J. Mater. Sci.*, **42**, [15], 6404–6411, (2007).
- 26 Chlup, Z., Hadraba, H., Slabáková, L., Drdlík, D., Dlouhý, I.: Fracture behaviour of alumina and zirconia thin layered laminate, *J. Eur. Ceram. Soc.*, **32**, [9], 2057–2061, (2012).
- 27 Nicolaidis, I., Gurauskis, J., Baudín, C., Moreno, R., Sánchez-Herencia, A.J.: Forming of ceramic laminates comprising thin layers of a few particles, *J. Am. Ceram. Soc.*, **91**, [7], 2124–2129, (2008).
- 28 Ferrari, B., Bueno, S., Baudín, C.: Consolidation of flaw-tolerant layered structures by the insertion of reactive layers, *Bol. Soc. Esp. Ceram.*, **48**, [5], 261–266, (2009).
- 29 Requena, J., Moreno, R., Moya, J.S.: Obtained by slip casting, *J. Am. Ceram. Soc.*, **13**, [72], 1511–1513, (1989).
- 30 Bermejo, R., Torres, Y., Baudín, C., Sánchez-Herencia, A.J., Pascual, J., Anglada, M., Llanes, L.: Threshold strength evaluation on an Al<sub>2</sub>O<sub>3</sub>-ZrO<sub>2</sub> multilayered system, *J. Eur. Ceram. Soc.*, **27**, [2–3], 1443–1448, (2007).
- 31 E.C. for Standardization, EN 623–2: Advanced technical ceramics - Monolithic ceramics - General and textural properties - Part 2: Determination of density and porosity, 1993.
- 32 E.C. for Standardization, EN 843–4: Advanced technical ceramics - Monolithic ceramics - Mechanical properties at room temperature - Part 4: Vickers, Knoop and Rockwell superficial hardness, 1994.
- 33 E.C. for Standardization, EN 843–1: Advanced technical ceramics - Monolithic ceramics - Mechanical properties at room temperature - Part 1: Determination of flexural strength, 10 (1995).
- 34 E.C. for Standardization, EN 843–5: Advanced technical ceramics - Mechanical properties of monolithic ceramics at room temperature - Part 5: Statistical analysis, 2006.
- 35 Ohji, T.: Testing and evaluation of mechanical properties, *Handbook of Advanced Ceramics*, 2<sup>nd</sup> Edition, Chapter 9.2, p. 633–650 (2013).
- 36 E.C. for Standardization, EN 658–3: Advanced technical ceramics - Mechanical properties of ceramic composites at room temperature - Part 3: Determination of flexural strength, 2002.
- 37 Chartier, T., Merle, D., Besson, J.L.: Laminar ceramic composites, *J. Eur. Ceram. Soc.*, **15**, [2], 101–107, (1995).
- 38 Tang, D., Lim, H.B., Lee, K.J., Lee, C.H., Cho, W.S.: Evaluation of mechanical reliability of zirconia-toughened alumina composites for dental implants, *Ceram. Int.*, **38**, [3], 2429–2436, (2012).
- 39 Casellas, D., Nagl, M.M., Llanes, L., Anglada, M.: Fracture toughness of alumina and ZTA ceramics: microstructural coarsening effects, *J. Mater. Process. Technol.*, **143–144**, [1], 148–152, (2003).
- 40 Spriggs, R.M., Vasilos, T.: Effect of grain size on transverse bend strength of alumina and magnesia, *J. Am. Ceram. Soc.*, **46**, [5], 224–228, (1963).
- 41 Hillman, C., Suo, Z., Lange, F.F.: Cracking of laminates subjected to biaxial tensile stresses, *J. Am. Ceram. Soc.*, **79**, 160, (1996).

